Exposure-Adjusted Bicycle Crash Risk Estimation and Safer Routing in Berlin

Eric Berger [*] **Edward Eichhorn** [*] **Liaisan Faidrakhmanova** [*] **Luise Grasl** [*] **Tobias Schnarr** [*]

Abstract

Accurately estimating the risk of bicycle crashes at street level requires consideration of both crash counts and cyclist exposure. However, exposure data from official counting stations is unavailable for most sections of the street network. This makes it difficult to identify the streets that are dangerous and should be avoided and prioritised for safety improvements. We therefore use Strava's bike trip data to estimate the relative crash risk across street segments and junctions in Berlin. These risk estimates identify those with a higher or lower than expected occurrence of crashes, and enable a routing algorithm to suggest lower-risk routes.

1. Introduction

Cycling is far from a safe endeavour. 92,882 bicycle crashes were recorded in 2024, including 441 fatalities - 16% of all traffic deaths that year (Destatis, 2025). Yet it is rarely clear which streets are most dangerous and thus should be avoided by cyclists or prioritised for safety improvements.

Quantifying street-level danger is non-trivial because simple crash counts confound risk with exposure. Streets with high exposure, i.e. high numbers of cyclists, tend to accumulate more crashes even when per-cyclist risk is low (Lücken, 2018). To reveal high-risk locations, crashes must be normalised by cyclist counts; otherwise, dangerous streets can remain hidden in dense urban networks (Uijtdewilligen et al., 2024). Unfortunately, comprehensive street-level cyclist counts are rarely available. Berlin, for example, provides hourly counts at selected locations via official counting stations, but their limited spatial coverage (20 stations for thousands of streets) makes them impractical for city-wide risk estimation (Senatsverwaltung für Mobilität, Verkehr, Klimaschutz und Umwelt).

We address this problem by using bike trip counts from the fitness-tracking app Strava. These have been used to predict official counting-station data (Dadashova et al., 2020) and we show that they can serve as a proxy for cyclist exposure. For all segments and junctions in Berlin's official cycling network, we estimate exposure-normalised relative risk, defined as the ratio of observed to expected crashes. Because Strava coverage can be sparse, we use empirical Bayes smoothing for estimation (Clayton & Kaldor, 1987), which stabilises estimates in low-exposure segments and junctions, and quantifies uncertainty. Additionally, building on these estimates, we introduce a routing algorithm that finds substantially lower-risk alternatives under a route-length constraint.

2. Data

Multiple datasets were used for risk estimation. Crash counts were taken from the *German Accident Atlas* (Destatis, 2025), which provides georeferenced locations of police-reported crashes where people were injured. We filtered the data to bicycle-related crashes within the city limits of Berlin. Cyclist exposure was approximated using the dataset by Kaiser et al. (2025b), which reports daily street-segment-level counts of bicycle trips recorded via the Strava app in Berlin from 2019 to 2023. Strava users are not representative of the general cycling population (they skew younger, male, and sport-oriented; Kaiser et al., 2025b). Therefore, we assess potential bias by comparing segment-level count shares in 2023 with official bicycle counter data from the city of Berlin (Senate Department for Urban Mobility, Transport, Climate Action and the Environment, 2024) for the subset of segments where both Strava data and official counts are available (Figure 2). Count shares correlate strongly ($r = .61$) and are overall well preserved in the Strava data. Segments on wide main streets (e.g., Karl-Marx-Allee) are overrepresented in the Strava data, likely reflecting faster rides that are more often tracked, whereas residential streets (e.g., Kollwitzstraße) are underrepresented, consistent with slower, local cycling that is less often tracked.

All datasets were combined into one dataframe and matched to the same street network and map projection. The network is represented as polyline segments with associated monthly exposure counts. We map crashes to the network

[*] Equal contribution. Correspondence to: Tobias Schnarr <tobias-marco.schnarr@student.uni-tuebingen.de>.

Project report for the "Data Literacy" course at the University of Tübingen, Winter 2025/26 (Module ML4201). Style template based on the ICML style files 2025. Copyright 2025 by the author(s).

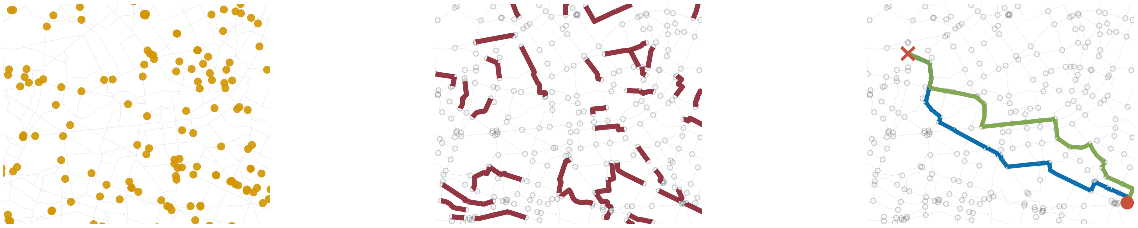

(a) Data

(b) Risk estimation

(c) Safety routing

Figure 1. **Safety-aware routing pipeline for the Berlin network.** Panels (a–c) are zoomed in for readability; see Section 3 for definitions and notation. (a) Police-recorded bicycle crashes in June 2021 (points) and street segments with measured cyclist exposure (lines). (b) Pooled segment-level relative crash risk estimated from all available data; high-risk segments in red correspond to values above the 90th percentile of relative risk; circles mark junctions (degree ≥ 3). (c) Shortest path (blue) versus a safer alternative (green) selected to reduce cumulative relative route risk under a distance-detour constraint. Filled circle and cross denote origin and destination, respectively.

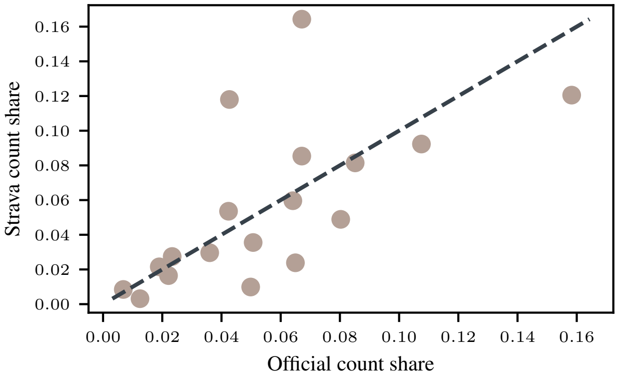

Figure 2. Consistency check between official bicycle counts and Strava-derived cyclist volumes at the street-segment level (2023). Points show segment-wise shares of total annual counts; the dashed line denotes equality between the two measures.

using nearest-segment assignment. Junctions are defined as nodes where at least three segments meet and crashes within a fixed radius are assigned to the nearest junction. Junction exposure is derived from the segment exposure (see Section 3 for details).

At monthly resolution, events are sparse: in a typical month, fewer than 5% of segments and 3% of junctions record at least one crash. We drop segments with zero recorded trips over at least one year and pool counts over the full period 2019–2023 for risk estimation. The dataset comprises 4,335 segments, 2,862 junctions, and 15,396 recorded bicycle crashes. The resulting segment- and junction-level relative risk estimates are used throughout the analysis and serve as inputs to the routing algorithm.

3. Methods

Crash, exposure, and risk measures. For each month t, let $C_{s,t}$ and $E_{s,t}$ denote the number of police-recorded bicycle crashes and measured cyclist exposure on street segment s. Junction crashes $C_{v,t}$ are defined as crashes within a fixed radius of junction v. Because a traversal typically contributes exposure to two incident segments, we approximate junction exposure by the half-sum of incident segment exposures,

$$E_{v,t} = \tfrac{1}{2} \sum_{s \in \mathcal{I}(v)} E_{s,t},$$

a common approach when turning movements are unavailable (Hakkert & Braimaister, 2002; Wang et al., 2020). For notational convenience, both street segments and junctions are indexed by a generic entity index i, with $A_{i,t}$ and $E_{i,t}$ denoting the corresponding crash and exposure quantities.

Under a no-special-risk baseline, monthly crash incidence is assumed proportional to exposure, yielding the expected number of crashes

$$\widehat{C}_{i,t} = C_{\cdot t} \frac{E_{i,t}}{E_{\cdot t}}, \qquad C_{\cdot t} = \sum_i C_{i,t}, \quad E_{\cdot t} = \sum_i E_{i,t},$$

where sums are taken jointly over all segments and junctions, defining a shared baseline. Because routing requires a pooled baseline risk estimate, crashes and baseline expectations are aggregated over the full period,

$$C_i = \sum_t C_{i,t}, \qquad \widehat{C}_i = \sum_t \widehat{C}_{i,t},$$

and the raw relative risk r_i^{raw} is $C_i / \widehat{C}_i$.

Empirical Bayes smoothing. Because many segments have low exposure and thus very small expected counts, the raw relative risk is highly variable. That is why we use Empirical Bayes smoothing to improve the risk estimates. This methods shrinks low-exposure estimates toward a baseline, while high-exposure estimates change little. Concretely, we assume a true relative risk r_i^{true} such that the observed count C_i follows a Poisson model with

$$C_i \mid r_i^{\text{true}} \sim \text{Poisson}(\widehat{C}_i \, r_i^{\text{true}}).$$

The Poisson distribution is natural for nonnegative event counts over a fixed time period under a baseline rate, and it yields $\mathbb{E}[C_i] = \widehat{C}_i$ when $r_i^{\text{true}} = 1$. To allow heterogeneity in relative risk beyond this baseline, we place a Gamma prior on r_i^{true} in the shape–rate parameterization,

$$r_i^{\text{true}} \sim \text{Gamma}(\alpha, \alpha),$$

which enforces $\mathbb{E}[r_i^{\text{true}}] = 1$ and has variance $\text{Var}(r_i^{\text{true}}) = 1/\alpha$ controlling the amount of shrinkage. The Gamma prior is also conjugate to the Poisson likelihood, giving a closed-form posterior

$$r_i^{\text{true}} \mid C_i, \widehat{C}_i \sim \text{Gamma}(C_i + \alpha, \; \widehat{C}_i + \alpha),$$

so posterior inference is simple and numerically stable. We estimate α from the data using method of moments (Morris, 1983), as

$$\widehat{\alpha} = \frac{\sum_i \widehat{C}_i^2}{\sum_i (C_i - \widehat{C}_i)^2 - \sum_i \widehat{C}_i}.$$

and use the posterior mean

$$\widehat{r}_i = \mathbb{E}[r_i^{\text{true}} \mid C_i, \widehat{C}_i] = \frac{C_i + \alpha}{\widehat{C}_i + \alpha}$$

as the smoothed relative risk. For small $\widehat{C}_i$, r_i is pulled toward 1, while for large $\widehat{C}_i$ it approaches the raw ratio $C_i/\widehat{C}_i$. Uncertainty is summarized by $(1 - \delta = 0.95)$ equal-tailed credible intervals from quantiles of the Gamma posterior.

Risk-weighted routing graph. Relative risk estimates are dimensionless and conditional on exposure. To obtain additive routing weights, we rescale relative risk by the pooled baseline crash rate,

$$\bar{\lambda} = \frac{C.}{E.}, \qquad C. = \sum_i C_i, \;\; E. = \sum_i E_i,$$

yielding the routing weight

$$w_i = \bar{\lambda} \, r_i.$$

We construct an undirected graph $G = (V, E)$ from the street network, where nodes correspond to segment endpoints and edges to street segments of length ℓ_e. Each edge e corresponds to a segment s and inherits its weight, $w_e = w_s$. Junction identifiers and weights are mapped to nodes via spatial snapping in a projected coordinate system, producing a single risk-annotated network.

Safety-aware routing. We compare shortest-distance routes with alternatives that reduce estimated crash risk under a bounded detour. The length of a route P is

$$L(P) = \sum_{e \in P} \ell_e.$$

To incorporate segment- and junction-level risk, the risk contribution of edge $e = (u, v)$ is defined as

$$\rho_e = w_e + \eta \, \frac{w_u + w_v}{2},$$

where w_u and w_v denote junction routing weights (zero for non-junction nodes), yielding an additive surrogate for cumulative route risk.

For an origin–destination pair, the baseline route P_{dist} minimizes $L(P)$. The safety-aware route is obtained by solving

$$\begin{aligned} P_{\text{safe}} = \arg\min_P R(P) = \sum_{e \in P} \rho_e \\ \text{s.t. } L(P) \le (1 + \varepsilon) \, L(P_{\text{dist}}), \end{aligned} \tag{1}$$

where ε is the allowable relative detour (Ehrgott, 2005). We approximate this constraint using a weighted-sum sweep: for $\lambda \in \Lambda$,

$$P(\lambda) = \arg\min_P \left(\sum_{e \in P} \rho_e + \lambda \sum_{e \in P} \ell_e \right),$$

and select the feasible route minimizing $R(P)$. Shortest paths are computed using Dijkstra's algorithm (Dijkstra, 1959).

Evaluation metrics. For each origin–destination pair, we report the relative length increase

$$\Delta_L = \frac{L(P_{\text{safe}}) - L(P_{\text{dist}})}{L(P_{\text{dist}})}$$

and the relative risk reduction

$$\Delta_R = \frac{R(P_{\text{dist}}) - R(P_{\text{safe}})}{R(P_{\text{dist}})}.$$

Pairs with $R(P_{\text{dist}}) = 0$ are excluded from Δ_R. We additionally report the expected number of avoided crashes,

$$\Delta_C = R(P_{\text{dist}}) - R(P_{\text{safe}}).$$

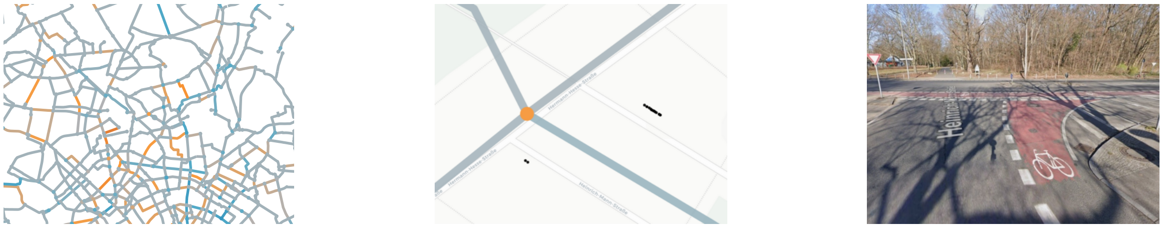

(a) Risk heatmap

(b) High-risk junction

(c) Street-level view

Figure 3. **Risk heatmap and detailed inspection of junction 2482.** The colors in panels (a)–(b) indicate $\log_{10}$-scaled risk values, ranging from low risk (-2) to high risk (2). (a) Section of the Strava bike network in Berlin with all computed road segments and junctions displayed. (b) Closer view of junction 2482 and the crashes (black dots) assigned to it, with risk values shown using the same color scale. (c) Street-level view of junction 2482 (Google, 2025), providing visual context for the observed risk.

4. Related Work

In accident risk estimation, a Hannover study combined police crash records with exposure estimates calibrated to official counters (Wage et al., 2022). However bicycle traffic was extrapolated from motorized transport data, poorly capturing actual cycling patterns. Other work calibrated crowdsourced GPS cycling data with count stations and showed that cyclist volumes strongly predict crash risk, though uncertainty of risk estimates on low-volume segments remained unexamined (Uijtdewilligen et al., 2024).

A separate research line addresses cyclist exposure where direct counts are unavailable. Supervised learning models estimate city-wide volumes by combining sparse counters with crowdsourced data and contextual features (Kaiser et al., 2025a). Graph neural networks estimate street-segment exposure under sparse sensor coverage (Kaiser et al., 2025b). These models achieved good predictive accuracy but required manual validation counts for calibration, which is not available in our case. However, these studies showed that crowdsourced Strava data correlates with official counting stations at segment level, supporting its direct use as exposure proxy.

To account for accident sparsity, some studies employed Poisson and Gamma count models (Lücken, 2018; Medeiros et al., 2021). These approaches handle zero-inflated crash data but exposure remained limited to city-level aggregation and weather-based reconstruction, lacking segment-level estimates required for routing applications.

5. Results

The estimated shrinkage parameter was small ($\widehat{\alpha} = 0.129$), resulting in limited regularization and a wide spread of relative risk estimates across segments and junctions. The segment and junctions are mapped with their estimated relative risks r as partly visualized in Figure 3 (a). Most elements show average or below-average risk: for 64.4% of the segments and 69.1% of the junctions $r = 1$ and for 17.6% of the segments and 25.8% of the junctions $r < 1$. Only 17.9% of the segments and 4.9% of the junctions show an elevated risk $r > 1$. Risk values range from 0.03 to 50.79 for segments and from 0.03 to 6.43 for junctions. Since the visualization highlights the segments and junctions with elevates risks, we pick one of them for further investigation and verification. For an exemplary high-risk location (junction 2482, $r = 6.43$), 22 crashes are assigned despite moderate traffic. Analyzing the crash data, we find all of them involved least one additional vehicle, predominantly (20) cars, and mainly occurred during turning or crossing maneuvers. Figure 3 (c) shows how car lanes cross the bicycle lane at this location.

We evaluated the algorithm using 1,000 random origin–destination pairs, comparing the shortest-path baseline against safest alternatives across a range of allowable detour and junction-risk constraints (Natera Orozco et al., 2020).

Table 1. Trade-off between path length increase and safety improvement under varying detour budgets (ε). Values are aggregated over all origin–destination pairs and reported as medians. The junction penalty weight is fixed to $\eta = 1$. Δ_L denotes the relative path length increase, Δ_R the relative reduction in expected crashes with respect to the shortest-path baseline, and Δ_C the absolute number of avoided expected crashes per 100,000 trips, reported as rounded integer counts.

ε	Δ_L (IQR)	Δ_R (IQR)	$\Delta_R > 0$	Δ_C (IQR)
0.00	0.000 (0.000)	0.000 (0.000)	0.037	0 (0)
0.05	0.007 (0.022)	0.101 (0.210)	0.767	39 (123)
0.10	0.015 (0.037)	0.147 (0.240)	0.841	61 (132)
0.15	0.024 (0.063)	0.169 (0.239)	0.873	71 (141)
0.20	0.041 (0.109)	0.192 (0.238)	0.901	83 (150)
0.30	0.091 (0.156)	0.237 (0.228)	0.928	104 (157)
0.40	0.137 (0.188)	0.262 (0.230)	0.944	112 (170)
0.50	0.165 (0.200)	0.281 (0.222)	0.948	121 (178)

Table 1 summarizes the trade-off between route length and exposure-adjusted crash risk under bounded detours. With a strictly bounded detour of only 5%, the median risk reduction ranges between 18.5% and 24.6%, depending on the junction penalty. Larger detours further increase these gains, reaching median risk reductions of 38%-43% at $\varepsilon = 0.2$. Safer route alternatives are available for the vast majority of trips (76%–92%) within the given detour budget. As the budget increases to 20%, over 90% of routes have a feasible, lower-risk alternative. Across all detour budgets, increasing η is associated with lower median risk reductions.

6. Discussion and Conclusion

This study combines street segment-level risk modeling with separate junction treatment, addressing sparse crash data and low-exposure segments through uncertainty quantification. Within a 10% route length increase, our method achieves a crash risk reduction of about one third—a modest detour for safer cycling.

However, limitations remain. Official data capture only personal injury crashes and suffer from under-reporting; during our study period, one researcher, Edward Eichhorn, experienced two bicycle accidents absent from official records. Additionally, cyclist exposure is approximated using Strava data, which represents a subset of specific cyclist types and likely overemphasizes routes popular within this community. Results therefore support relative risk comparisons and routing decisions rather than absolute crash probability estimates.

The approach transfers to cities with crash data, a routable street network, and an exposure proxy. All code and supplementary materials are available at https://github.com/ytobiaz/data_literacy.

Contribution Statement

Explain here, in one sentence per person, what each group member contributed. For example, you could write: Max Mustermann collected and prepared data. Gabi Musterfrau and John Doe performed the data analysis. Jane Doe produced visualizations. All authors will jointly wrote the text of the report. Note that you, as a group, a collectively responsible for the report. Your contributions should be roughly equal in amount and difficulty.

References

Clayton, D. and Kaldor, J. Empirical bayes estimates of age-standardized relative risks for use in disease mapping. *Biometrics*, 43(3):671, September 1987. ISSN 0006-341X. doi: 10.2307/2532003. URL http://dx.doi.org/10.2307/2532003.

Dadashova, B., Griffin, G. P., Das, S., Turner, S., and Sherman, B. Estimation of average annual daily bicycle counts using crowdsourced strava data. *Transportation Research Record: Journal of the Transportation Research Board*, 2674(11):390–402, September 2020. ISSN 2169-4052. doi: 10.1177/0361198120946016. URL http://dx.doi.org/10.1177/0361198120946016.

Destatis. German accident atlas, 2025. URL https://unfallatlas.statistikportal.de/. Retrieved January 14 2026.

Dijkstra, E. W. A note on two problems in connexion with graphs. *Numerische Mathematik*, 1(1):269–271, 1959. ISSN 0945-3245. doi: 10.1007/bf01386390. URL http://dx.doi.org/10.1007/BF01386390.

Ehrgott, M. *Multicriteria Optimization*, volume 491 of *Lecture Notes in Economics and Mathematical Systems*. Springer, Berlin, Heidelberg, 2005. ISBN 978-3-540-21398-7. URL https://doi.org/10.1007/3-540-27659-9.

Google. Google Street View: Junction Heinrich-Mann-Straße/Hermann-Hesse-Straße Berlin, 2025. URL https://maps.app.goo.gl/pxxqfSwW8Rbtu6AZ8.

Hakkert, A. S. and Braimaister, L. The uses of exposure and risk in road safety studies. Technical Report R-2002-12, SWOV Institute for Road Safety Research, Leidschendam, The Netherlands, 2002. URL http://www.swov.nl/rapport/R-2002-12.pdf.

Kaiser, S. K., Klein, N., and Kaack, L. H. From counting stations to city-wide estimates: data-driven bicycle volume extrapolation. *Environmental Data Science*, 4, 2025a. ISSN 2634-4602. doi: 10.1017/eds.2025.5. URL http://dx.doi.org/10.1017/eds.2025.5.

Kaiser, S. K., Rodrigues, F., Azevedo, C. L., and Kaack, L. H. Spatio-temporal graph neural network for urban spaces: Interpolating citywide traffic volume, 2025b. URL https://arxiv.org/abs/2505.06292.

Lücken, L. On the variation of the crash risk with the total number of bicyclists. *European Transport Research Review*, 10(2):33, 2018. doi: 10.1186/s12544-018-0305-9. URL https://doi.org/10.1186/s12544-018-0305-9.

Medeiros, R. M., Bojic, I., and Jammot-Paillet, Q. Spatiotemporal variation in bicycle road crashes and traffic volume in berlin: Implications for future research, planning, and network design. *Future Transportation*, 1(3):686–706, 2021. ISSN 2673-7590. doi: 10.3390/futuretransp1030037. URL https://www.mdpi.com/2673-7590/1/3/37.

Morris, C. N. Parametric empirical bayes inference: Theory and applications. *Journal of the American Statistical Association*, 78(381):47–55, 1983. ISSN 1537-274X. doi: 10.1080/01621459.1983.10477920. URL http://dx.doi.org/10.1080/01621459.1983.10477920.

Natera Orozco, L. G., Battiston, F., Iñiguez, G., and Szell, M. Data-driven strategies for optimal bicycle network growth. *Royal Society Open Science*, 7(12):201130, 2020. ISSN 2054-5703. doi: 10.1098/rsos.201130. URL http://dx.doi.org/10.1098/rsos.201130.

Senate Department for Urban Mobility, Transport, Climate Action and the Environment. Radverkehrszählstellen – jahresbericht 2023, 2024. URL https://www.berlin.de/sen/uvk/_assets/verkehr/verkehrsplanung/radverkehr/weitere-radinfrastruktur/zaehlstellen-und-fahrradbarometer/bericht_radverkehr_2023.pdf?ts=1752674590. Stand: 31.05.2024 (Berlin, Mai 2024). Accessed: 2026-02-01.

Senatsverwaltung für Mobilität, Verkehr, Klimaschutz und Umwelt. Zählstellen und fahrradbarometer: Fahrradverkehr in zahlen. URL https://www.berlin.de/sen/uvk/mobilitaet-und-verkehr/verkehrsplanung/radverkehr/weitere-radinfrastruktur/zaehlstellen-und-fahrradbarometer/.

Uijtdewilligen, T., Ulak, M. B., Wijlhuizen, G. J., Bijleveld, F., Geurs, K. T., and Dijkstra, A. Examining the crash risk factors associated with cycling by considering spatial and temporal disaggregation of exposure: Findings from four dutch cities. *Journal of Transportation Safety & Security*, 16(9):945–971, 2024.

doi: 10.1080/19439962.2023.2273547. URL https://doi.org/10.1080/19439962.2023.2273547.

Wage, O., Bienzeisler, L., and Sester, M. Risk analysis of cycling accidents using a traffic demand model. *The International Archives of the Photogrammetry, Remote Sensing and Spatial Information Sciences*, XLIII-B4-2022:427–434, 2022. doi: 10.5194/isprs-archives-XLIII-B4-2022-427-2022. URL https://isprs-archives.copernicus.org/articles/XLIII-B4-2022/427/2022/.

Wang, K., Zhao, S., and Jackson, E. Investigating exposure measures and functional forms in urban and suburban intersection safety performance functions using generalized negative binomial - p model. *Accident Analysis & Prevention*, 148:105838, 2020. ISSN 0001-4575. doi: https://doi.org/10.1016/j.aap.2020.105838. URL https://www.sciencedirect.com/science/article/pii/S0001457520316584.